REPORT

TBCE Mutations Cause Early-Onset Progressive Encephalopathy with Distal Spinal Muscular Atrophy

Antonella Sferra,[1,11] Gilbert Baillat,[2,11] Teresa Rizza,[1] Sabina Barresi,[1] Elisabetta Flex,[3] Giorgio Tasca,[1] Adele D'Amico,[1] Emanuele Bellacchio,[1] Andrea Ciolfi,[1,4] Viviana Caputo,[5] Serena Cecchetti,[6] Annalaura Torella,[7,8] Ginevra Zanni,[1] Daria Diodato,[1] Emanuela Piermarini,[1] Marcello Niceta,[1] Antonietta Coppola,[9] Enrico Tedeschi,[10] Diego Martinelli,[1] Carlo Dionisi-Vici,[1] Vincenzo Nigro,[7,8] Bruno Dallapiccola,[1] Claudia Compagnucci,[1] Marco Tartaglia,[1,12,*] Georg Haase,[2,12] and Enrico Bertini[1,12,*]

Tubulinopathies constitute a family of neurodevelopmental/neurodegenerative disorders caused by mutations in several genes encoding tubulin isoforms. Loss-of-function mutations in *TBCE*, encoding one of the five tubulin-specific chaperones involved in tubulin folding and polymerization, cause two rare neurodevelopmental syndromes, hypoparathyroidism-retardation-dysmorphism and Kenny-Caffey syndrome. Although a missense mutation in *Tbce* has been associated with progressive distal motor neuronopathy in the *pmn/pmn* mice, no similar degenerative phenotype has been recognized in humans. We report on the identification of an early-onset and progressive neurodegenerative encephalopathy with distal spinal muscular atrophy resembling the phenotype of *pmn/pmn* mice and caused by biallelic *TBCE* mutations, with the c.464T>A (p.Ile155Asn) change occurring at the heterozygous/homozygous state in six affected subjects from four unrelated families originated from the same geographical area in Southern Italy. Western blot analysis of patient fibroblasts documented a reduced amount of TBCE, suggestive of rapid degradation of the mutant protein, similarly to what was observed in *pmn/pmn* fibroblasts. The impact of *TBCE* mutations on microtubule polymerization was determined using biochemical fractionation and analyzing the nucleation and growth of microtubules at the centrosome and extracentrosomal sites after treatment with nocodazole. Primary fibroblasts obtained from affected subjects displayed a reduced level of polymerized α-tubulin, similarly to tail fibroblasts of *pmn/pmn* mice. Moreover, markedly delayed microtubule re-polymerization and abnormal mitotic spindles with disorganized microtubule arrangement were also documented. Although loss of function of TBCE has been documented to impact multiple developmental processes, the present findings provide evidence that hypomorphic *TBCE* mutations primarily drive neurodegeneration.

Tubulinopathies are a family of severe neurodevelopmental disorders caused by mutations in multiple genes encoding tubulin isoforms (e.g., *TUBA1A* [MIM: 602529], *TUBA8* [MIM: 605742], *TUBB2B* [MIM: 612850], *TUBB3* [MIM: 602661], and *TUBB5* [MIM: 191130]), with defective neuronal migration and cerebral cortex malformation representing their major features.[1] Inactivating mutations in *TBCE* (tubulin folding cofactor E [MIM: 604934]), encoding one of the five tubulin-specific chaperones involved in tubulin folding and polymerization, are known to cause two rare neurodevelopmental syndromes, hypoparathyroidism-retardation-dysmorphism syndrome (HRDS [MIM: 241410]), which is characterized by congenital hypoparathyroidism, intellectual disability, facial dysmorphism, and extreme growth failure, and Kenny-Caffey syndrome type 1 (KCS1 [MIM: 244460]), which overlaps HRDS but exhibits osteosclerosis and recurrent bacterial infections as additional features.[2] All reported children with HRDS and KCS1 but one originate from inbred families of Middle Eastern origin (Saudi and Israeli pedigrees) and carry a recurrent homozygous in-frame deletion (c.155_166delGCCACGAAGGGA [p.Ser52_Gly55del]) in *TBCE* (GenBank: NM_001079515.2) resulting in virtually absent protein level.[2,3] Two additional mutations, both truncating (c.66_67delAG [p.Val23fs48*] and c.T1113A [p.Cys371*]), have been reported in a compound heterozygous state in a Belgian pedigree with two siblings manifesting features of HRDS.[2] More recently, microtubule-disrupting mutations in tubulin genes have also been shown to trigger neurodegeneration, as illustrated by *TUBA4A* (MIM: 191110) and *TUBB4A* (MIM: 602662) mutations underlying amyotrophic lateral sclerosis (MIM: 616208) and hypomyelinating leukodystrophy associated with progressive spastic dystonic tetraplegia (MIM: 612438), respectively.[4,5] Similarly, a missense *Tbce* mutation predicting the p.Trp524Gly amino acid substitution has been associated with progressive distal motor neuronopathy in *pmn/pmn* mice,[6,7] but no similar phenotype has so far

[1]Genetics and Rare Diseases Research Division, Ospedale Pediatrico Bambino Gesù, 00146 Rome, Italy; [2]Institut de Neurosciences de la Timone, UMR 7289 CNRS Aix-Marseille University, 13005 Marseille, France; [3]Department of Hematology, Oncology and Molecular Medicine, Istituto Superiore di Sanità, 00161 Rome, Italy; [4]Centro di Ricerca per gli alimenti e la nutrizione, CREA, 00178 Rome, Italy; [5]Department of Experimental Medicine, Università La Sapienza, 00161 Rome, Italy; [6]Department of Cell Biology and Neurosciences, Istituto Superiore di Sanità, 00161 Rome, Italy; [7]Department of Biochemistry, Biophysics and General Pathology, Seconda Università degli Studi di Napoli, 80138 Naples, Italy; [8]Telethon Institute of Genetics and Medicine, 80078 Pozzuoli, Italy; [9]Department of Neuroscience, Reproductive and Odontostomatological Sciences, Università degli Studi di Napoli Federico II, 80131 Naples, Italy; [10]Department of Advanced Biomedical Sciences, Università degli Studi di Napoli Federico II, 80131 Naples, Italy
[11]These authors contributed equally to this work
[12]These authors contributed equally as the senior investigators in this project
*Correspondence: marco.tartaglia@opbg.net (M.T.), bertini@opbg.net (E.B.)
http://dx.doi.org/10.1016/j.ajhg.2016.08.006.

been reported in humans. Here, we report on the identification of an early-onset neurodegenerative encephalopathy resembling the phenotype of *pmn*/*pmn* mice, caused by biallelic *TBCE* mutations, with the c.464T>A missense change (p.Ile155Asn) occurring at the heterozygous/homozygous state in all affected subjects. We also show that the mutation results in a reduced amount of TBCE and that defective TBCE function in primary fibroblasts is associated with a lowered amount of polymerized α-tubulin, markedly delayed microtubule re-polymerization, and abnormal mitotic spindle morphology. Consistent with what we had previously been observed in *pmn*/*pmn* mice, the present findings demonstrate that hypomorphic TBCE function primarily drives neurodegeneration.

Six individuals from four apparently unrelated families originating from the same geographical area (metropolitan area of Naples in Campania, Southern Italy, and Ischia Island, just off the coast) were included in the study. Clinical features are schematically listed in Table 1 and summarized in the Supplemental Case Reports. Clinical data and biological material collection and storage were attained from the participating families after written informed consent was obtained, and the study was approved by the Ethical Committees of the participating centers. Genomic DNA and total RNA was isolated from peripheral blood leukocytes, using standard protocols. We originally performed whole-exome sequencing (WES) on genomic DNA obtained from subjects 1544334 and 2518864 (Figure 1). Both subjects had been followed at the Ospedale Pediatrico Bambino Gesù, Rome, and shared a neurodegenerative disorder characterized by early-onset slowly progressive distal motor neuropathy resembling distal spinal muscular atrophy (SMA) with bilateral foot drop associated to spasticity and cerebellar ataxia. They did not exhibit dysmorphia or growth defects. Muscle biopsy confirmed neurogenic muscle atrophy, and brain magnetic resonance imaging (MRI) documented cerebellar atrophy (Figure 1). In both cases, we used a trio-based (proband and unaffected parents) strategy. Exome capture was carried out using SureSelect Human All Exon v.4 (Agilent), and WES data analysis was performed using an in-house implemented pipeline, as previously reported.[8–10] Paired-end reads were aligned to the human genome (UCSC GRCh37/hg19) with the Burrows-Wheeler Aligner (BWA v.0.7.10). Presumed PCR duplicates were discarded using Picard tools' MarkDuplicates. GATK tools were used for realignment of sequences encompassing indels and for base quality recalibration.[11] SNPs and small indels were identified by means of the GATK's HaplotypeCaller used in gVCF mode, followed by family-level joint genotyping and phasing, according to GATK's latest best practices. Called variants were filtered to retain variants with quality > 100 and quality-by-depth score > 1.5. High-quality variants were then filtered against public databases (dbSNP142 and ExAC v.0.3) to retain novel and clinically associated variants, and annotated variants with unknown frequency or having MAF < 0.1% and occurring with a frequency < 2% in an in-house database including frequency data from approximately 600 population-matched WES. SnpEff toolbox (v.4.1)[12] was used to predict the functional impact of variants, which were filtered to retain only those located in exons with any effect on the coding sequence, and splice site regions (−3 to +8 with respect to exon-intron junctions). Functional annotation of variants was performed with SnpEff v.4.1 and dbNSFP v.2.8,[12,13] and their functional impact was analyzed by Combined Annotation Dependent Depletion (CADD) v.1.3 and dbNSFP Support Vector Machine (SVM) v.3.0 algorithms.[14,15] For sequencing statistics, see Table S1. Data annotation predicted 13,541 and 13,484 high-quality variants having functional impact (i.e., non-synonymous and splice site changes) in subjects 1544334 and 2518864, respectively. Among them, 356 and 350 clinically associated, private, and low/unknown frequency variants were retained for further analyses. Because family 1 had documented consanguinity, filtering was first directed to identify genes shared by the probands having variants compatible with a recessive inheritance models. We identified only one gene, *TBCE*, satisfying the filtering criteria. Specifically, subject 1544334 (family 1) was homozygous for the c.464T>A missense change (p.Ile155Asn) and subject 2518864 was a compound heterozygote for the same nucleotide substitution and the truncating c.1076delC (p.Leu360Ter) change. Sanger sequencing confirmed both variants and segregation in each family (Figure S1). No gene with a putative de novo change was shared by the two probands, and none of the genes with putative de novo variants in each individual was functionally linked to processes relevant to neurodegeneration (Table S1), strongly pointing to *TBCE* as the gene implicated in the disorder. Mutation scan of the *TBCE* coding sequence was successively performed on two monozygotic twins (subjects 00997847 and 00997844) of a third family originating from the same geographical area. Both individuals exhibited MRI profiles and an overall clinical phenotype overlapping that of the two previous cases, and Sanger sequencing allowed us to identify homozygosity for the recurrent c.464T>A change (Figure S1). Finally, interrogation of the Telethon Institute of Genetics and Medicine WES variant database allowed us to identify an additional sibling pair homozygous for the c.464T>A missense substitution (Figure S1). In that family, WES had been performed to identify the genetic cause of an unsolved apparently recessive neurodegenerative disorder characterized by spastic tetraparesis, optic atrophy, and abnormal brain MRI (cerebellar and brainstem atrophy, corpus callosum hypotrophy, and white matter hyperintensity with iron deposition in the globus pallidus and substantia nigra) resembling a pattern of neurodegeneration with brain iron accumulation (NBIA [MIM: 234200]) (Figure 2). Clinical reassessment of the two affected subjects revealed clinical features matching the disorder characterizing the previously identified subjects homozygous/compound heterozygous for the *TBCE* c.464T>A change. Remarkably,

Table 1. Clinical Features of Subjects with Biallelic Mutations in *TBCE*

Affected Subjects	1544334	2518864	00997847	00997844	VN_X3359	VN_3360
Family	1	2	3	3	4	4
Gender	male	male	male	male	female	male
Year of birth	2007	2009	2000		1996	2001
Inheritance	simplex case	simplex case	simplex case		familial	familial
Consanguinity	yes	no	no		no	no
Pregnancy, delivery, neonatal period	normal, weight at birth 3,360 g at 39th week of gestation	normal, weight at birth 3,490 g at 38th week of gestation	normal, weight 3,030 g at 37th week gestation	normal, weight 2,570 g at 37th week gestation	normal, weight at birth 2,600 g at 38th week of gestation	normal, weight at birth 3,250 g at 39th week of gestation
Initial motor & cognitive development	neonatal period normal	abnormal	neonatal period normal		neonatal period normal	normal until 8 months
Age at presentation	around 4–5 months of age	at birth	around 4–5 months of age		14 months	8 months
Signs of presentation	hypotonia and developmental delay in the first year of life	hypotonia and developmental delay in the first year of life	hypotonia and developmental delay in the first year of life		spasticity and developmental delay in the first year of life	spasticity and developmental delay in the first year of life
Signs of regression	distal amyotrophy, ataxia, spasticity	distal amyotrophy, ataxia, spasticity	distal amyotrophy, ataxia, spasticity		distal amyotrophy, spastic tetraparesis, optic atrophy	distal amyotrophy, spastic paraparesis, optic atrophy
Outcome						
Age (years)	6	6	15	15	20	15
Motor function	able to sit	never able to sit	lost the ability to sit	lost the ability to sit	lost the ability to sit	lost the ability to sit
Cognitive level	mildly affected	moderately affected	moderately affected	moderately affected	severely affected	severely affected
Speech and language	able to speak, dysarthria	not able to speak	able to speak, severe dysarthria	able to speak, severe dysarthria	not able to speak	severe dysarthria
TBCE mutations[a]	c.463T>A (p.Ile155Asn), c.463T>A (p.Ile155Asn)	c.463T>A (p.Ile155Asn), c.1076delC (p.Leu360Ter)	c.463T>A (p.Ile155Asn), c.463T>A (p.Ile155Asn)		c.463T>A (p.Ile155Asn), c.463T>A (p.Ile155Asn)	c.463T>A (p.Ile155Asn), c.463T>A (p.Ile155Asn)

[a]Both variants have been reported with low recurrence in public databases (c.464T>A, rs780472451, 0.0000082/1, ExAC; c.1076delC, rs750781063, 0.00002/3, ExAC). Mutations are annotated according to GenBank: NM_001079515.2 (NP_001072983.1).

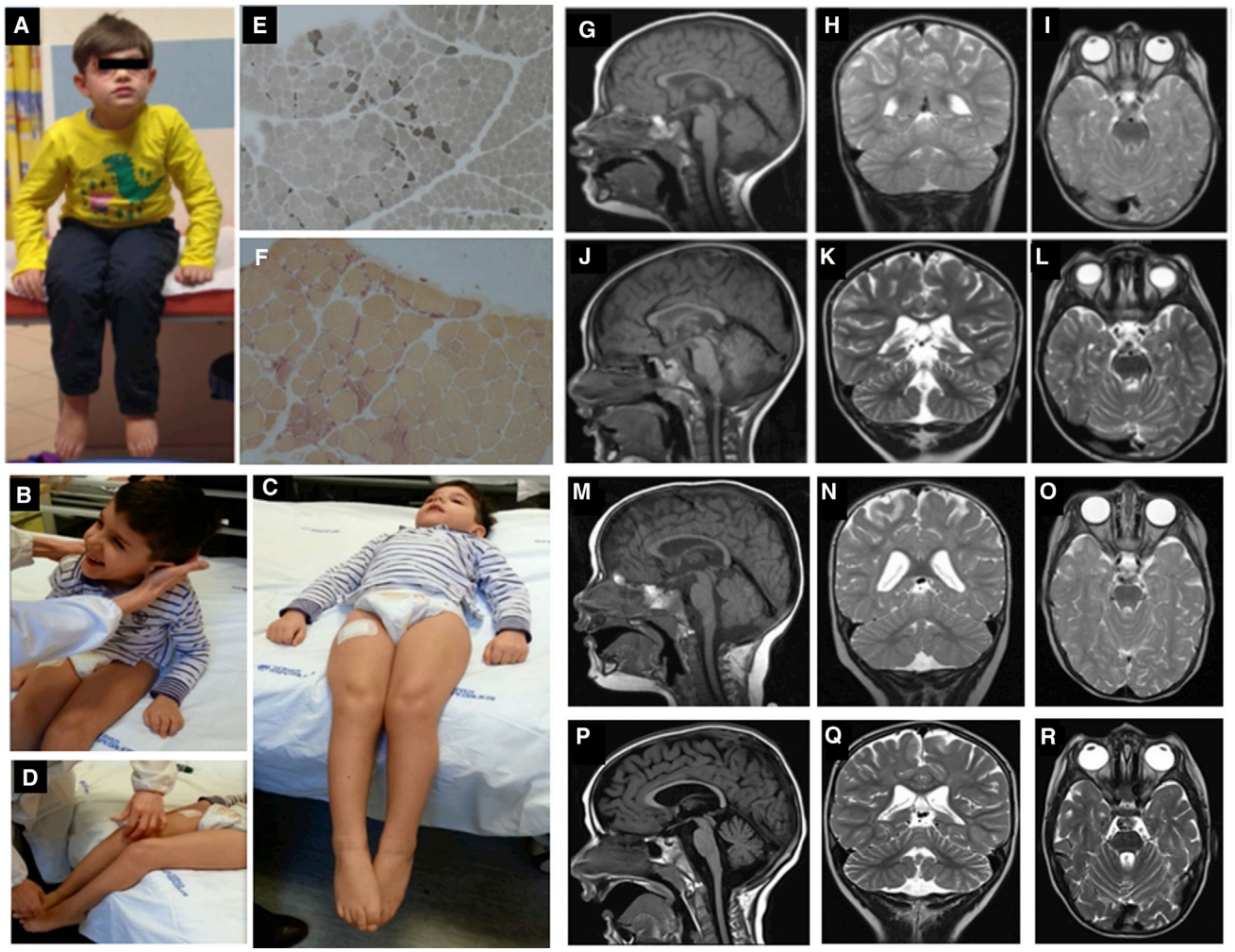

Figure 1. ***TBCE*** **Mutations Cause Early-Onset Encephalopathy with Distal Spinal Muscular Atrophy**
Clinical features of subjects 1544334 (A) and 2518864 (B–D); muscle biopsy of 1544334 stained with ATPase 4.3 showing fiber type grouping and scattered atrophic angulated fibers (E) and atrophic angulated fibers that are denervated because positively stained with non-specific esterase (F); brain MRIs of subjects 1544334 (G–I, at 2 years; J–L, at 3 years) and 2518864 (M–O, at 1 year; P–R, at 2 years). Note the hypoplasia of corpus callosum and the cerebellar atrophy with prominent folia (K, Q).

similar to the other case subjects, the family was from Pozzuoli and Mergellina, located in the Naples metropolitan area, along the coast near Ischia Island. Parents were not consanguineous. WES data statistics are reported in Table S1.

All affected subjects were homozygous or compound heterozygous for the c.464T>A missense change and were from the same geographical area, strongly suggesting a founder effect. The variant has recently been reported in the ExAC database (rs780472451) with an overall estimated frequency of 0.000008 (1/121,411, information on the ethnic origin of the carrier not available). Genotyping of 400 unrelated and apparently unaffected individuals from the Naples metropolitan area by ARMS-PCR (primers and PCR conditions available on request) failed in identifying any allele carrying the variant (0–0.0025, 95% confidence interval). Based on the informative variants identified by WES to flank the c.464T>A change, the genomic region encompassing the disease-causing variant shared by the three families was estimated to cover approximately 1.3 Mb (chr1: 235,357,303–236,687,580). To more precisely define the size of the shared fragment, eight microsatellite markers covering the *TBCE* locus were selected, and the four trios were genotyped using an ABI PRISM 3500 Sequencer and the GeneMapper 4.0 software (Applied Biosystems). Reconstruction of the haplotypes allowed us to refine the length of the shared genomic region, which spanned approximately 0.5 Mb (Table S2), confirming the identity by descent of the c.464T>A missense variant.

All individuals homozygous or compound heterozygous for the c.464T>A variant in *TBCE* shared a strikingly homogeneous phenotype with clinical signs of progressive neurodegeneration, associated with normal calcium/phosphate metabolism and absence of repeated infections (Table 1 and Supplemental Case Reports), clearly differing from HRDS and KCS. By contrast, their clinical features were reminiscent of the *pmn/pmn* mouse,[16] in which the progressive motor neuronopathy, hindlimb atrophy, and

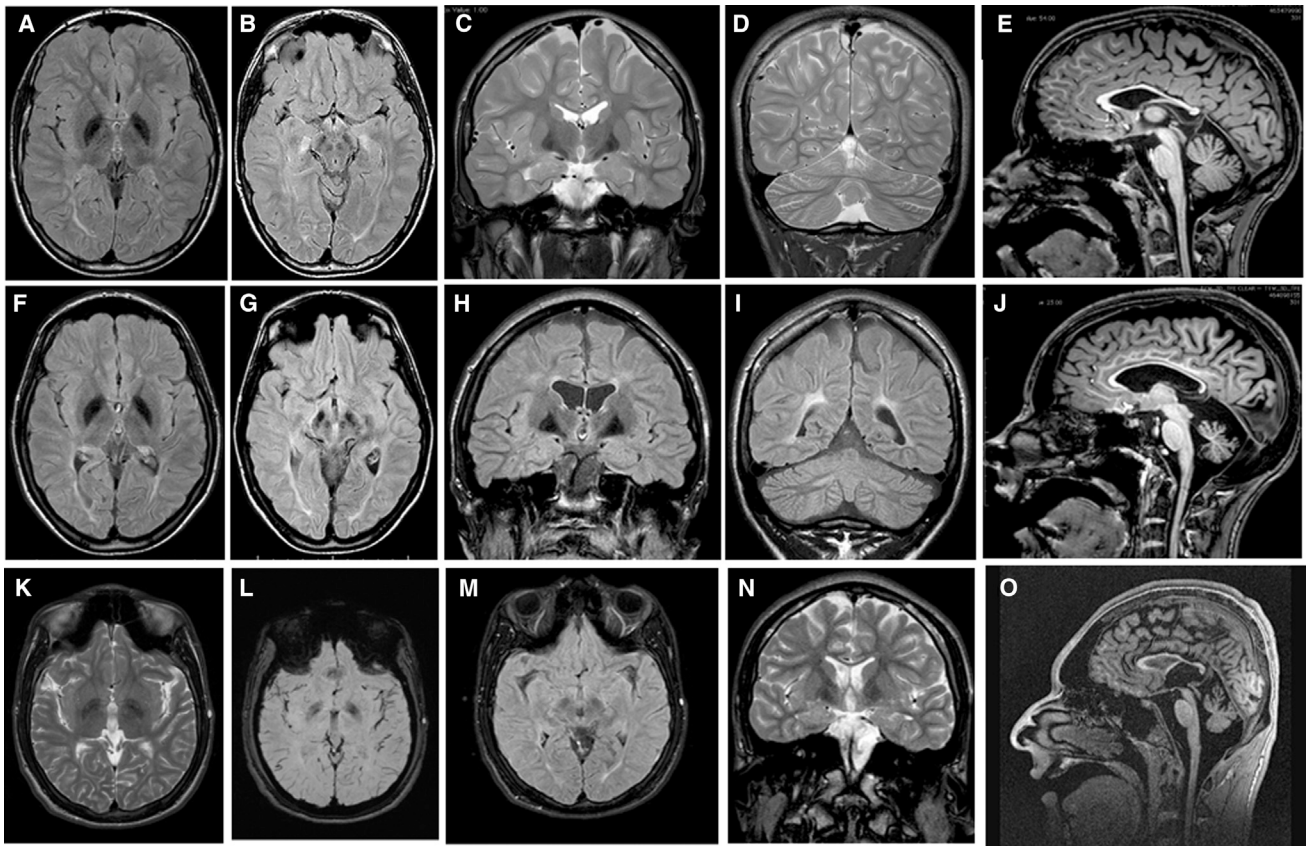

Figure 2. *TBCE* Mutations Cause a Pattern of Neurodegeneration with Brain Iron Accumulation in the Second Decade of Life of Affected Individuals

(A–J) Brain MRIs of subjects VN_X5360 (A–E, performed at age 13 years) and VN_X3359 (F–J, performed at age 17 years). Axial FLAIR-weighted images shown in (A), (B), (F), and (G); coronal T2-weighted images shown in (C) and (D); T1-weighted sagittal images shown in (E) and (J); (A), (B), (F), (G), (H), and (I) are FLAIR-weighted images. Note T2 or FLAIR hypointense areas corresponding to globi pallidi, substantia nigra, and mesencephalic red nuclei in both siblings, indicating abnormal iron deposits.

(K–O) Brain MRIs of subject 00997847 performed at age 16 years. Axial T2-weighted image shown in (K); a T2 coronal weighted image shown in (N); two axial T2* relaxation-weighted images documenting the presence of iron shown in (L) and (M); and a sagittal T1-weighted image shown in (O). The hypointense areas detected in T2-weighted images correspond to the increased iron for age accumulated at the level of the globi pallidi and substantia nigra.

reduced brain size is caused by a missense substitution in the same gene (p.Trp524Gly) documented to partially impair TBCE stability and function.[6,7]

TBCE is a 527-amino-acid-long protein characterized by an N-terminal CAP-Gly domain, a motif mediating protein binding to α-tubulin, followed by nine tandemly arranged leucine-rich repeat (LRR) motifs, and a C-terminal ubiquitin-like domain possibly implicated in α-tubulin degradation via the proteasome (Figure S1).[17,18] Ile155 is a highly conserved residue across orthologs (Figure S1) and is located within the LRR domain. A homology model of the protein region spanning the nine LRRs (residues 123–348) was generated on the basis of the available LRR domain structure of internalin H (PDB: 1H6U), using the program Swiss-PdbViewer 4.1;[19] loops were modeled with MODELER v.9.13.[20] The generated model fitted well with the established structure of these motifs[21] and localized the affected residue in the hydrophobic core stabilizing the second LRR motif (Figure 3A). At the same position, the introduction of the hydrophilic asparagine was predicted to perturb dramatically the structure of the motif and the overall folding of the LRR domain. Since LRR domains are functional modules that mediate protein-protein interaction, this amino acid substitution was expected to affect TBCE function or the overall TBCE structure and protein stability. To verify the latter hypothesis, the level of TBCE was evaluated by western blot analysis in skin fibroblasts obtained from affected subjects 1544334 and 2518864 and four healthy control subjects. Fibroblasts were lysed with RIPA buffer containing protease inhibitors cocktail (Roche), and 30 μg of total proteins were separated on a 4%–12% Bis-Tris gel (Invitrogen) and transferred to polyvinylidene difluoride membrane (Amersham). After blocking, membranes were incubated with anti-TBCE (Novus) (1:1,000) and anti-GAPDH (Sigma) (1:10,000) antibodies, the latter used to normalize samples loading. After washing, membranes were incubated with the secondary antibodies (Jackson ImmunoResearch), and immunoreactive bands were visualized using Lite Ablot Extend Long Lasting Chemiluminescent Substrate

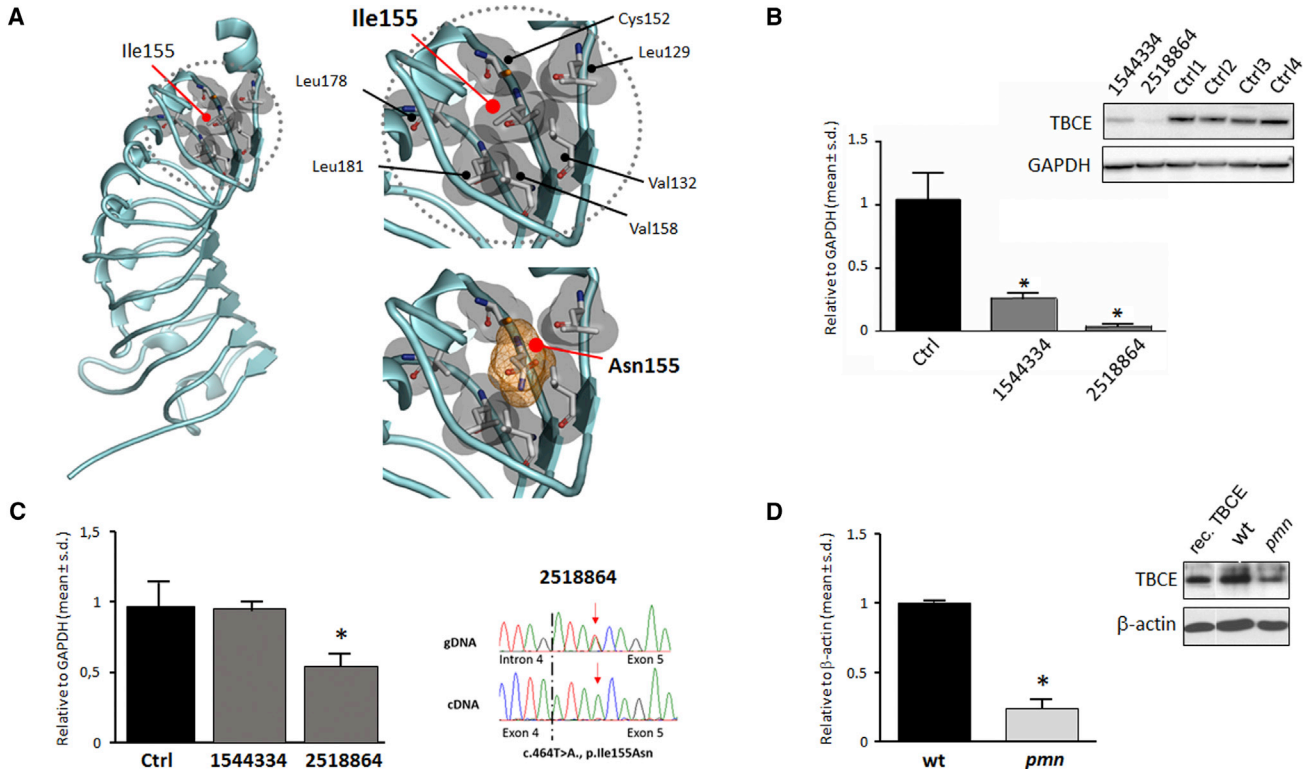

Figure 3. Predicted Structural Impact of the p.Ile155Asn Substitution, and Consequence of *TBCE* Mutations on mRNA and Protein Levels

(A) Homology model of the TBCE leucine-rich repeat (LRR) domain (residues 123–348, GenBank: NP_001072983.1). Ile155 with surrounding hydrophobic residues contributes to the hydrophobic core required for proper folding of the domain. Introduction of Asn is predicted to disrupt the intramolecular binding network stabilizing the LRR structure.

(B) Western blot (WB) analysis documenting reduced TBCE levels in fibroblasts from affected subjects. Data are presented as means ± SD, *$p < 0.05$ (Mann-Whitney test).

(C) Real-time qRT-PCR showing reduced expression level of *TBCE* mRNA in fibroblasts from subject 2518864. *$p < 0.05$ (Mann-Whitney test). Such reduced level of the transcript is caused by transcript decay of the allele carrying the truncating c.1076delC variant, as documented by Sanger sequencing of *TBCE* cDNA showing solely the transcript with the c.464T>A missense change.

(D) WB analysis demonstrating reduced levels of Tbce in tail fibroblasts from the *pmn/pmn* mouse ($Tbce^{Trp524Gly}$); recombinant protein (rec. TBCE) is also reported. Data are presented as means ± SD, *$p < 0.01$ (Mann-Whitney test).

(Euroclone). Western blot analysis documented a significantly reduced amount of TBCE in fibroblasts from affected individuals compared to control cells (Figure 3B), suggestive of rapid degradation of the TBCE mutant. Of note, reduction in TBCE levels was more accentuated in fibroblasts from subject 2518864, who was compound heterozygote for the p.Ile155Asn and p.Leu360Ter changes. To compare the levels of *TBCE* mRNA among samples, total RNA from cell lysates was isolated using TRIzol solution (Invitrogen) and 1 μg RNA was reverse transcribed with the SuperScript First-Strand Synthesis system (Invitrogen), using random hexamers as primers. *TBCE* mRNA expression levels were determined by quantitative real-time PCR using an ABI PRISM 7000 Sequence Detection System (Applied Biosystems) and Power SYBR Green I dye chemistry. Assays were performed in triplicate, with *GAPDH* as internal controls, and documented a reduction to half of normal of *TBCE* mRNA in fibroblasts from subject 2518864 compared to what was observed in individual 1544334 and control cells (Figure 3C). Consistent with this finding, the frameshift variant was undetectable at the mRNA level, as determined by cDNA Sanger sequencing (Figure 3C), indicating nonsense-mediated RNA decay. A similar reduction in Tbce levels was documented in fibroblasts (Figure 3D) of *pmn/pmn* mice. Overall these data indicated that TBCE levels in fibroblasts of subjects with isolated neurodegenerative disease is preserved, in part, in sharp contrast with the extremely reduced or completely absent level of the protein documented in HRDS and KCS.[3,22]

TBCE is required for the folding of α-tubulin, α/β-tubulin dimerization, and subsequent heterodimer polymerization into microtubules, which are major components of the cytoskeleton.[23,24] To explore the impact of the two *TBCE* mutations on microtubule polymerization, we first determined the levels of total, soluble, and polymerized α-tubulin in fibroblasts of affected and control subjects, using biochemical fractionation. Total, soluble, and polymerized tubulins from fibroblast lysates were separated by centrifugation (16,000 × *g*, 30 min, room temperature) as previously described.[25] Proteins were solubilized by heating in Laemmli buffer, separated on 10% SDS-PAGE,

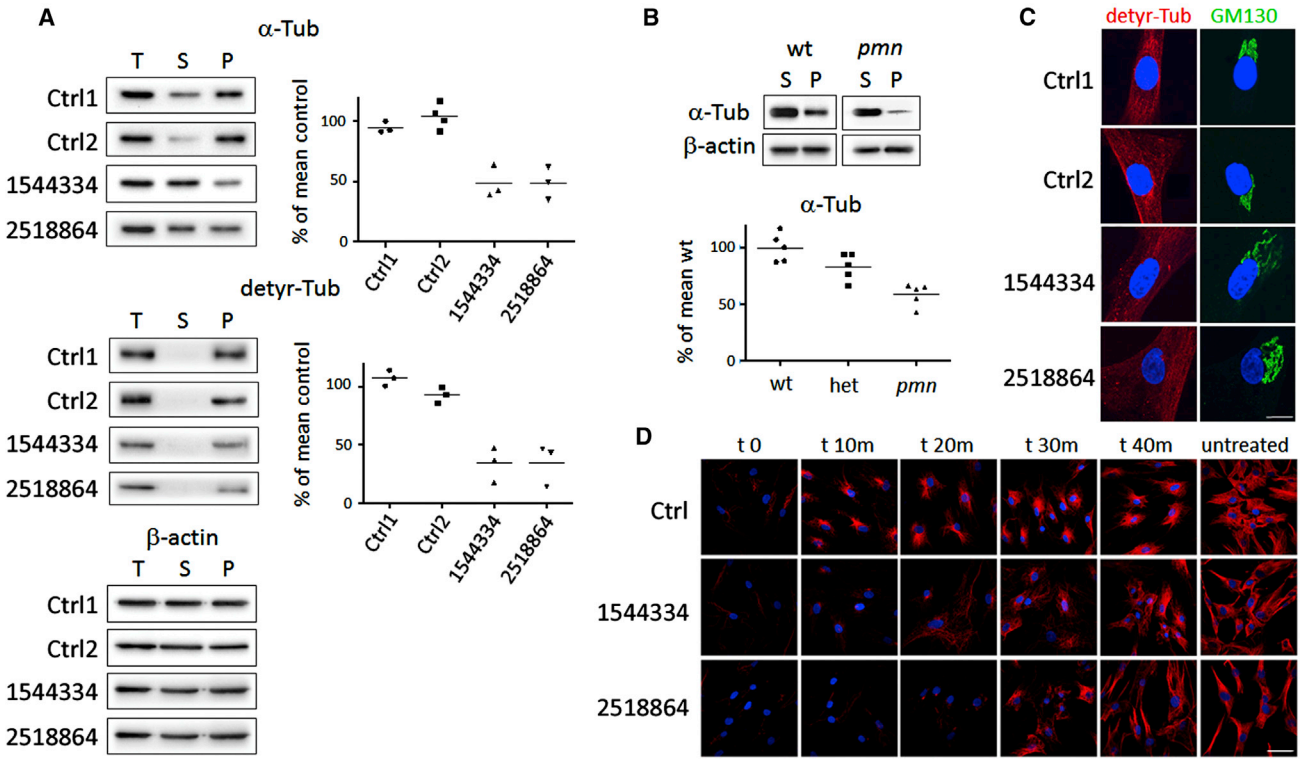

Figure 4. Defective Microtubule Polymerization in Subjects with Homozygous/Heterozygous *TBCE* c.464T>A Missense Change and in *pmn*/*pmn* Mice

(A) Western blot (WB) analyses showing total (T), soluble (S), and polymerized (P) α-tubulin (above), detyrosinated tubulin (middle), and β-actin (below) in fibroblasts from affected individuals (1544334, 2518864) and in control cells (Ctrl1, Ctrl2). Diagrams (right) show reduced fractions of polymerized α-tubulin and detyrosinated tubulin in fibroblasts of affected subjects. In both comparisons, differences were statistically significant by Mann-Whitney test ($p < 0.01$).

(B) WB analyses showing reduced amount of polymerized α-tubulin (P) in fibroblasts from *pmn*/*pmn* mice compared to control fibroblasts (wt). Differences were statistically significant by Mann-Whitney test ($p < 0.01$).

(C) Immunofluorescence analysis documenting loss of microtubules containing detyrosinated tubulin (detyr-Tub) in fibroblasts of affected subjects. Note that detyrosinated microtubules (red) in control fibroblasts are closely associated with the GM130-stained Golgi apparatus (green), while the Golgi apparatus in fibroblasts carrying mutated *TBCE* alleles appears to have lost compaction. Nuclei are DAPI stained (blue). Scale bar represents 10 μm.

(D) Immunofluorescence analyses showing reduced re-polymerization of microtubules (labeled for α-tubulin, red) after nocodazole treatment in fibroblasts from subjects 1544334 and 2518864, as compared to control cells (Ctrl). Nuclei are labeled with DAPI (blue). Scale bar represents 20 μm.

and transferred on membranes, which were immunoblotted with antibodies against α-tubulin (Sigma) (1:5,000), detyrosinated tubulin (a kind gift of Dr. A. Andrieux, INSERM, Grenoble, France) (1:10,000), and β-actin (TuJ1, Babco) (1:10,000). The level of total α-tubulin did not significantly differ among cells (Figure 4A). By contrast, the amount of polymerized α-tubulin was significantly reduced in fibroblasts from affected subjects compared to control cells (Figure 4A), in line with what was observed in tail fibroblasts of *pmn*/*pmn* mice (Figure 4B). Moreover, significantly reduced levels of detyrosinated α-tubulin, a marker of stable and long-lived microtubules in neurons, were also noted (Figure 4A), indicating again a reduced microtubule stability in fibroblasts with biallelic mutations in *TBCE*.

We hypothesized that defective TBCE function might alter microtubule nucleation and dynamics. To verify this hypothesis, synchronized fibroblasts from individuals with mutated *TBCE* alleles and unaffected controls were cultured in Dulbecco's Modified Eagle Medium supplemented with 10% FBS, seeded on coverslips, and allowed to attach for 24 hr. Cells were treated with the microtubule-disrupting drug nocodazole (Sigma) (10 μM, 35 min at 37°C), and microtubule regrowth was analyzed after drug washout by confocal microscopy analysis, in time-course experiments, after fibroblasts were fixed, and immunostained for α-tubulin (Sigma) and with DAPI (Life Technologies). Cultures were visualized with a confocal microscope Fluoview FV1000 (Olympus) and images were acquired with the software FV10-ASW v.2.0. In control fibroblasts, microtubules began to polymerize efficiently as early as 10 min after nocodazole washout, and extended polymerized structures were well formed at 30 min (Figure 4C). By contrast, microtubule re-polymerization appeared markedly delayed in fibroblasts from affected subjects; microtubules were also less abundant and strongly disorganized in both early and late stages of re-polymerization. Such altered dynamics appeared particularly

pronounced in fibroblasts with compound heterozygosity for the p.Ile155Asn and p.Leu360Ter changes, consistent with the more profound reduction of TBCE levels.

TBCE is concentrated at the Golgi membrane in an Arf1-regulated manner and facilitates both nucleation rates and polymerization speed of Golgi-derived microtubules.[26] Immunofluorescence of synchronized primary fibroblasts was performed to visualize tubulin polymerization using antibodies against detyrosinated tubulin (1:1,000), as a marker of microtubules, and the Golgi membrane, using an anti-GM130 antibody (Becton Dickinson) (1:300). A decreased level of detyrosinated tubulin was observed in fibroblasts from affected subjects (Figure 4D), in line with the previously collected data and the reported loss of Golgi-derived microtubules in motor neurons of *pmn/pmn* mice.[26] Of note, such reduced nucleation of microtubules was associated with a decreased compaction of the Golgi apparatus (Figure 4D).

Microtubules are a key cytoskeletal component of the mitotic apparatus, and their centrosomal nucleation coordinates formation and dynamics of the mitotic spindle during mitosis. To explore the occurrence of altered microtubule spindle organization, confocal microscopy analysis of synchronized fibroblasts from subjects with mutated *TBCE* alleles and unaffected individuals was performed. Fixed cells were stained with pericentrin (Abcam), γ-tubulin (Sigma), and α-tubulin (Abcam) antibodies, followed by the appropriate secondary antibodies (Invitrogen) and DAPI to visualize chromosomes. An abnormal mitotic morphology and disorganized mitotic microtubules were observed; spindles appeared asymmetric and unrefined and exhibited an irregular aster structure (Figure S2), documenting the impact of the hypomorphic defect in TBCE on mitotic spindle formation and organization.

The level of α/β-tubulin heterodimers as well as their polymerization and depolymerization at the microtubule ends are tightly controlled in cells to guarantee proper dynamics of this cytoskeletal component. Since microtubules control multiple neuronal processes, including cell division, migration, function, and survival,[23] neurons are particularly vulnerable to altered microtubule dynamics. In this report, we provide evidence that defective TBCE function underlies a recessive early-onset neurodegenerative disorder and is associated with perturbed microtubule dynamics characterized by decreased and delayed microtubule polymerization. TBCE is a tubulin-binding cofactor required for the formation of α/β-tubulin heterodimers, microtubule polymerization, and also tubulin scavenging. Virtually complete loss of TBCE function has previously been identified to underlie two clinically related developmental disorders, HRDS and KCS1.[2,3] In contrast, hypomorphic Tbce function has specifically been reported to cause a neurodegenerative disorder in *pmn/pmn* mice due to retrograde dying back of motor axons and degeneration of motor neuron cell bodies.[6,7,16,27] The present data provide evidence of a similar neurodegenerative phenotype in humans resulting from defective TBCE function.

Consistent with the presently observed reduced nucleation of microtubules at the Golgi apparatus and decreased compaction of the Golgi apparatus, previous observations in *pmn/pmn* mice and TBCE-depleted motor neurons have documented that defective TBCE function impairs microtubule polymerization at the Golgi apparatus, leading to defective trafficking of COPI vesicles and Golgi fragmentation, which interestingly represents one of the earliest pathological features of degenerating motor neurons in amyotrophic lateral sclerosis.[28,29] In sharp contrast, HRDS and KCS are syndromic conditions mainly affecting multiple developmental processes and growth, with no sign of early-onset and progressive neurodegeneration, and in particular no sign of functional alterations involving upper and lower motor neurons. At the moment we have no explanation for this remarkable phenotypic difference. This picture has similarities with the phenotypic heterogeneity associated with mutations in *ASAH1* (MIM: 613468), encoding N-acylsphingosine amidohydrolase 1, in which hypomorphic defects have been linked to childhood SMA associated with progressive myoclonic epilepsy (SMA-PME [MIM: 159950]), a rare autosomal-recessive phenotype restricted to the central nervous system generally starting with lower motor neuron disease,[29] while a different class of mutations dramatically affecting catalytic activity of the enzyme results in Farber disease (MIM: 228000), a lysosomal storage disease characterized by severe motor and intellectual disability, early-onset subcutaneous lipogranulomata, painful and progressively deformed joints, and hoarseness of the voice.

Another remarkable clinical aspect of TBCE-related neurodegeneration is the MRI pattern resembling NBIA that was documented in the four older affected sibs in their second decade (subjects VN_X3359, VN_X5360, 00997847, and 00997844). We suppose that this pattern might represent a feature evolving with age, possibly appearing during the second decade of life. This pattern is unexpected because iron accumulation has not been reported among the neuropathological features of the *pmn/pmn* mouse.[16] Although additional observations are needed to confirm this unexpected association, this finding suggests a critical role of cytoskeletal components in the complex cellular processes implicated in iron homeostasis in the brain.[30]

Overall, we describe a distal motor neuropathy, spastic ataxia, and juvenile-onset brain iron accumulation caused by biallelic mutations in *TBCE* overlapping the phenotype of the *pmn/pmn* mouse, a well-known model of motor neuron disease. Expanding beyond the previously documented impact of abolished TBCE function on developmental processes and growth, our findings indicate a stringent requirement of TBCE specifically for neuronal survival and function.

Supplemental Data

Supplemental Data include case reports, two figures, and two tables and can be found with this article online at http://dx.doi.org/10.1016/j.ajhg.2016.08.006.

Acknowledgments

We are grateful to the participating families. This work was supported in part by grants from Fondazione Bambino Gesù (Vite Coraggiose to M.T.), Bulgari (GeneRare to B.D.), Ministero della Salute (RC2015 and RC2016 to M.N., M.T., and E. Bertini), and Agence Nationale de la Recherche (to G.H.).

Received: May 18, 2016
Accepted: August 9, 2016
Published: September 22, 2016

Web Resources

Burrows-Wheeler Aligner, http://bio-bwa.sourceforge.net/
CADD, http://cadd.gs.washington.edu/
Chimera, http://www.cgl.ucsf.edu/chimera
dbNSFP v.2.0, https://sites.google.com/site/jpopgen/dbNSFP
dbSNP, http://www.ncbi.nlm.nih.gov/projects/SNP/
ExAC Browser, http://exac.broadinstitute.org/
GATK Best Practices, https://www.broadinstitute.org/gatk/guide/best-practices
GenBank, http://www.ncbi.nlm.nih.gov/genbank/
NCBI Gene, http://www.ncbi.nlm.nih.gov/gene
OMIM, http://www.omim.org/
Picard, http://broadinstitute.github.io/picard/
RCSB Protein Data Bank, http://www.rcsb.org/pdb/home/home.do

References

1. Bahi-Buisson, N., Poirier, K., Fourniol, F., Saillour, Y., Valence, S., Lebrun, N., Hully, M., Bianco, C.F., Boddaert, N., Elie, C., et al.; LIS-Tubulinopathies Consortium (2014). The wide spectrum of tubulinopathies: what are the key features for the diagnosis? Brain *137*, 1676–1700.
2. Parvari, R., Hershkovitz, E., Grossman, N., Gorodischer, R., Loeys, B., Zecic, A., Mortier, G., Gregory, S., Sharony, R., Kambouris, M., et al.; HRD/Autosomal Recessive Kenny-Caffey Syndrome Consortium (2002). Mutation of TBCE causes hypoparathyroidism-retardation-dysmorphism and autosomal recessive Kenny-Caffey syndrome. Nat. Genet. *32*, 448–452.
3. Courtens, W., Wuyts, W., Poot, M., Szuhai, K., Wauters, J., Reyniers, E., Eleveld, M., Diaz, G., Nöthen, M.M., and Parvari, R. (2006). Hypoparathyroidism-retardation-dysmorphism syndrome in a girl: A new variant not caused by a TBCE mutation–clinical report and review. Am. J. Med. Genet. A. *140*, 611–617.
4. Smith, B.N., Ticozzi, N., Fallini, C., Gkazi, A.S., Topp, S., Kenna, K.P., Scotter, E.L., Kost, J., Keagle, P., Miller, J.W., et al.; SLAGEN Consortium (2014). Exome-wide rare variant analysis identifies TUBA4A mutations associated with familial ALS. Neuron *84*, 324–331.
5. Simons, C., Wolf, N.I., McNeil, N., Caldovic, L., Devaney, J.M., Takanohashi, A., Crawford, J., Ru, K., Grimmond, S.M., Miller, D., et al. (2013). A de novo mutation in the β-tubulin gene TUBB4A results in the leukoencephalopathy hypomyelination with atrophy of the basal ganglia and cerebellum. Am. J. Hum. Genet. *92*, 767–773.
6. Martin, N., Jaubert, J., Gounon, P., Salido, E., Haase, G., Szatanik, M., and Guénet, J.L. (2002). A missense mutation in Tbce causes progressive motor neuronopathy in mice. Nat. Genet. *32*, 443–447.
7. Bommel, H., Xie, G., Rossoll, W., Wiese, S., Jablonka, S., Boehm, T., and Sendtner, M. (2002). Missense mutation in the tubulin-specific chaperone E (Tbce) gene in the mouse mutant progressive motor neuronopathy, a model of human motoneuron disease. J. Cell Biol. *159*, 563–569.
8. Cordeddu, V., Redeker, B., Stellacci, E., Jongejan, A., Fragale, A., Bradley, T.E., Anselmi, M., Ciolfi, A., Cecchetti, S., Muto, V., et al. (2014). Mutations in ZBTB20 cause Primrose syndrome. Nat. Genet. *46*, 815–817.
9. Kortüm, F., Caputo, V., Bauer, C.K., Stella, L., Ciolfi, A., Alawi, M., Bocchinfuso, G., Flex, E., Paolacci, S., Dentici, M.L., et al. (2015). Mutations in KCNH1 and ATP6V1B2 cause Zimmermann-Laband syndrome. Nat. Genet. *47*, 661–667.
10. Niceta, M., Stellacci, E., Gripp, K.W., Zampino, G., Kousi, M., Anselmi, M., Traversa, A., Ciolfi, A., Stabley, D., Bruselles, A., et al. (2015). Mutations impairing GSK3-mediated MAF phosphorylation cause cataract, deafness, intellectual disability, seizures, and a Down syndrome-like facies. Am. J. Hum. Genet. *96*, 816–825.
11. McKenna, A., Hanna, M., Banks, E., Sivachenko, A., Cibulskis, K., Kernytsky, A., Garimella, K., Altshuler, D., Gabriel, S., Daly, M., and DePristo, M.A. (2010). The Genome Analysis Toolkit: a MapReduce framework for analyzing next-generation DNA sequencing data. Genome Res. *20*, 1297–1303.
12. Cingolani, P., Platts, A., Wang, L., Coon, M., Nguyen, T., Wang, L., Land, S.J., Lu, X., and Ruden, D.M. (2012). A program for annotating and predicting the effects of single nucleotide polymorphisms, SnpEff: SNPs in the genome of *Drosophila melanogaster* strain w1118; iso-2; iso-3. Fly (Austin) *6*, 80–92.
13. Liu, X., Jian, X., and Boerwinkle, E. (2013). dbNSFP v2.0: a database of human non-synonymous SNVs and their functional predictions and annotations. Hum. Mutat. *34*, E2393–E2402.
14. Kircher, M., Witten, D.M., Jain, P., O'Roak, B.J., Cooper, G.M., and Shendure, J. (2014). A general framework for estimating the relative pathogenicity of human genetic variants. Nat. Genet. *46*, 310–315.
15. Dong, C., Wei, P., Jian, X., Gibbs, R., Boerwinkle, E., Wang, K., and Liu, X. (2015). Comparison and integration of deleteriousness prediction methods for nonsynonymous SNVs in whole exome sequencing studies. Hum. Mol. Genet. *24*, 2125–2137.
16. Schmalbruch, H., Jensen, H.J., Bjaerg, M., Kamieniecka, Z., and Kurland, L. (1991). A new mouse mutant with progressive motor neuronopathy. J. Neuropathol. Exp. Neurol. *50*, 192–204.
17. Serna, M., Carranza, G., Martín-Benito, J., Janowski, R., Canals, A., Coll, M., Zabala, J.C., and Valpuesta, J.M. (2015). The structure of the complex between α-tubulin, TBCE and TBCB reveals a tubulin dimer dissociation mechanism. J. Cell Sci. *128*, 1824–1834.
18. Voloshin, O., Gocheva, Y., Gutnick, M., Movshovich, N., Bakhrat, A., Baranes-Bachar, K., Bar-Zvi, D., Parvari, R., Gheber, L., and Raveh, D. (2010). Tubulin chaperone E binds microtubules and proteasomes and protects against misfolded protein stress. Cell. Mol. Life Sci. *67*, 2025–2038.
19. Guex, N., and Peitsch, M.C. (1997). SWISS-MODEL and the Swiss-PdbViewer: an environment for comparative protein modeling. Electrophoresis *18*, 2714–2723.

20. Sali, A., and Blundell, T.L. (1993). Comparative protein modelling by satisfaction of spatial restraints. J. Mol. Biol. *234*, 779–815.
21. Bella, J., Hindle, K.L., McEwan, P.A., and Lovell, S.C. (2008). The leucine-rich repeat structure. Cell. Mol. Life Sci. *65*, 2307–2333.
22. Tian, G., Huang, M.C., Parvari, R., Diaz, G.A., and Cowan, N.J. (2006). Cryptic out-of-frame translational initiation of TBCE rescues tubulin formation in compound heterozygous HRD. Proc. Natl. Acad. Sci. USA *103*, 13491–13496.
23. Kapitein, L.C., and Hoogenraad, C.C. (2015). Building the neuronal microtubule cytoskeleton. Neuron *87*, 492–506.
24. Sanders, A.A., and Kaverina, I. (2015). Nucleation and dynamics of Golgi-derived microtubules. Front. Neurosci. *9*, 431.
25. Minotti, A.M., Barlow, S.B., and Cabral, F. (1991). Resistance to antimitotic drugs in Chinese hamster ovary cells correlates with changes in the level of polymerized tubulin. J. Biol. Chem. *266*, 3987–3994.
26. Bellouze, S., Schäfer, M.K., Buttigieg, D., Baillat, G., Rabouille, C., and Haase, G. (2014). Golgi fragmentation in pmn mice is due to a defective ARF1/TBCE cross-talk that coordinates COPI vesicle formation and tubulin polymerization. Hum. Mol. Genet. *23*, 5961–5975.
27. Schaefer, M.K., Schmalbruch, H., Buhler, E., Lopez, C., Martin, N., Guenet, J.L., and Haase, G. (2007). Progressive motor neuronopathy: a critical role of the tubulin chaperone TBCE in axonal tubulin routing from the Golgi apparatus. J. Neurosci. *27*, 8779–8789.
28. Gonatas, N.K., Stieber, A., Mourelatos, Z., Chen, Y., Gonatas, J.O., Appel, S.H., Hays, A.P., Hickey, W.F., and Hauw, J.J. (1992). Fragmentation of the Golgi apparatus of motor neurons in amyotrophic lateral sclerosis. Am. J. Pathol. *140*, 731–737.
29. Mourelatos, Z., Gonatas, N.K., Stieber, A., Gurney, M.E., and Dal Canto, M.C. (1996). The Golgi apparatus of spinal cord motor neurons in transgenic mice expressing mutant Cu,Zn superoxide dismutase becomes fragmented in early, preclinical stages of the disease. Proc. Natl. Acad. Sci. USA *93*, 5472–5477.
30. Arber, C.E., Li, A., Houlden, H., and Wray, S. (2016). Review: Insights into molecular mechanisms of disease in neurodegeneration with brain iron accumulation: unifying theories. Neuropathol. Appl. Neurobiol. *42*, 220–241.

The American Journal of Human Genetics, Volume *99*

Supplemental Data

TBCE Mutations Cause Early-Onset Progressive Encephalopathy with Distal Spinal Muscular Atrophy

Antonella Sferra, Gilbert Baillat, Teresa Rizza, Sabina Barresi, Elisabetta Flex, Giorgio Tasca, Adele D'Amico, Emanuele Bellacchio, Andrea Ciolfi, Viviana Caputo, Serena Cecchetti, Annalaura Torella, Ginevra Zanni, Daria Diodato, Emanuela Piermarini, Marcello Niceta, Antonietta Coppola, Enrico Tedeschi, Diego Martinelli, Carlo Dionisi-Vici, Vincenzo Nigro, Bruno Dallapiccola, Claudia Compagnucci, Marco Tartaglia, Georg Haase, and Enrico Bertini

CASE REPORTS

Clinical features of the subjects included in the study are summarized below and are schematically listed in Table 1.

Subject 1544334. This subject, originating from the island of Ischia, Naples, was born on 2007 from first cousin parents, and was firstly examined at the age of 18 months because of delayed motor and cognitive development. At birth, weight was 3,240 g, and length was 50 cm. He was able to sit without support but was not able to walk, although moved in quadrupeds. Neurological examination documented signs of spasticity in his legs, and the brain MRI showed a thin corpus callosum with no additional abnormalities. The Griffith Mental Developmental scale scored 43 QG indicating moderate delay with ES -8.5 months. At 4 years, he was not able to walk, and could stand with support only for a short time because of spasticity, unsteadiness, and a bilateral foot drop. No fasciculations were detected. He was able to speak, using simple sentences, and had dysarthria. At 8 years, weight was 29 kg (50th-75th centile) and height was 125 cm (25th-50th centile).

Subject 2518864. This subject (b. 2009), also originating from the island of Ischia, was born from healthy and not related parents. Birth occurred when he was at the 38^{th} week of gestation (weight: 3,490 g; length: 35 cm; OFC: 35 cm). Hypotonia and poor antigravity movements were noticed during the first months of life, and severe developmental delay was noticed during the first year. The child was not able to control his head by age 10 months, and has never been able to sit. Neurological examination at 5 years showed an alert child who was not able to speak; he had limb weakness, which was more severe in lower limbs; sitting was possible with support. At 5 years, weight was 16 kg (25th centile), and height was 108 cm (50th centile). There was a bilateral foot drop, and bilateral foot clonus. Fasciculations were not detected. Swallowing was possible with difficulty.

Subjects 00997847 and 00997844. The two individuals (b. 2000) were monozygotic twins born from unrelated and healthy parents originating from Naples. Weight at birth (37 weeks of gestation without complications) was 3,030 and 2,570 g, respectively. The twin sibs had a clinical history of delayed milestones already in the first year of life. They achieved ability to sit alone at age 12 months, and were able to stand with support around age 18 months. At 2 years, they were able to speak in sentences but with severe dysarthria. The disease slowly progressed in both sibs, who manifested spasticity in their legs, ataxia, and distal amyotrophy of upper and lower limbs, without evidence of fasciculations. Both twins loosed autonomous sitting position by the age of 5 years. Around the age of 8 years, they started to have swallowing disturbances with drooling. Now, at 15 years, they are both wheelchair bond, showing severe distal amyotrophy of hands and feet, ataxia, spasticity, and scoliosis.

Subject VN_X3359. This young lady is the first child of healthy unrelated parents, both originating from the metropolitan area of Naples. She was born in 1996 after an uneventful pregnancy, and was

delivered at the 38th weeks of gestation by Caesarian section due to membrane disruption. Her birth weight was 2,060 g. Her developmental milestones were reported within normal epochs until the age of 12 months when she was noted to stand with difficulties. From the age of 14 months, developmental regression was observed together with progressive hypertonia of the four limbs. In the following months, distal amyotrophy and optic atrophy appeared. Moreover, she lost the ability to pronounce the few fords she had learned. At the age of 12 years, she also started suffering from frequent simple partial seizures. The patient came to our attention at the age of 18 years because of therapy resistant seizures. These were mainly characterized by focal hemiclonic convulsions, sometimes occurring in clusters. Neurological examination showed severe intellectual disability, absent language, spastic tetraparesis with distal amyotrophy, abnormal eyes movement, strabismus. The physical examination showed severe scoliosis.

Subject VN_X5360. This subject is the younger sibling of VN_X3359. He was born in 2001 after uneventful pregnancy, and was delivered at the 39th weeks of gestation with a birth weight of 3,250 g. His developmental milestones were reported normal until the age of 8 months when the child started exhibiting difficulties in holding his head and progressive hypertonia of the four limbs. Ataxia, dysarthria and optic atrophy subsequently appeared. He came under our attention at the age of 13 when he was wheelchair bound. At that time the neurological examination showed severe intellectual disability, dysarthria, spastic tetraparesis with distal amyotrophy, abnormal eye movements and strabismus. The physical examination showed severe scoliosis. He has never suffered from seizures; however the electroencephalography showed epileptiform abnormalities over the left parieto-occipital regions.

Additional laboratory investigations. Since inactivating mutations of *TBCE* had previously been documented to cause severe defects in calcium and phosphorus (Ca/P) metabolism and growth failure, extensive endocrinological and metabolic examinations were performed in all subjects. In 1544334, 2518864, 00997847 and 00997844, levels of Ca/P were within normal values. In 1544334, at 7 years, an extensive endocrinological investigation of the hypothalamic-pituitary-adrenal axis showed only a slightly reduced response to GHRF and reduced release of cortisol. Similarly, extensive endocrinological investigation in subjects 2518864, 00997847 and 00997844 yielded normal results. Importantly, no feature compatible with a diagnosis of hypoparathyroidism was documented; similarly, growth was normal in all individuals. Overall, the clinical phenotype in all subjects clearly differed from what observed in both hypoparthyroidism-retardation-dysmorphism (MIM 241410) and Kenny-Caffey syndrome (MIM 244460).

In subject 1544334, multimodal evoked potentials (VEPs) were normal. Motor nerve conduction velocity of lower limbs (45 m/sec in the right peroneal nerve) was normal with a markedly

reduced compound muscle action potential (CMAP) amplitude (0,5 mVs in the right extensor digitorum brevis muscle), while sensory conduction velocity and sensory action potential (SAP) of the sural nerve were normal (8 mVs, 48 m/sec), indicating a motor neuropathy. Similarly, in 2518864, multimodal electrophysiological examination showed normal brainstem evoked responses (BAERs), somatosensory evoked potentials (SSEPs) as well as sensory and motor nerve conduction velocities; CMAP had low amplitudes (0.4 mVs) in the extensor digitorum brevis of feet; visual evoked responses were slightly delayed with normal ERG. Electromyography (EMG) was performed in all subjects and showed clear neurogenic features in distal and proximal muscles of their legs characterized by polyphasic motor units, with increased duration, high amplitude, and recruitment with increased firing rate. Fibrillation potentials were detected only in distal muscles, while fasciculations were never detected. The muscle biopsy showed signs of denervation atrophy in subjects 1544334, 2518864, 00997847 and 00997844, the electrophysiological multimodal examination showed delayed VEPs, and BAERs, while SSEPs evoked from lower limbs were normal.

In all individuals, the ophthalmological evaluation documented bilateral optic atrophy. The brain MRI of subject 1544334 (2 years) showed a thin corpus callosum. A following MRI (3 years) showed a moderate global cerebellar atrophy and confirmed a thin corpus callosum. Subjects 2518864, 00997847 and 00997844 exhibited similar MRI features. In siblings VN_X3359 and VN_X5360, brain and spine MRIs performed at 17 (VN_X3359) and 13 (VN_X5360) years showed atrophy of the cerebellum, which was prominent in the vermis, and hypoplasia of the dorsal spine, together with white matter T2 hyperintensity in the posterior periventricular areas, T1 hypointensity areas in the pallidum and substantia nigra suggesting iron deposition, and marked corpus callosum hypoplasia. Similarly, in twin subjects 00997847 and 00997844, a MRI was performed at age 16 years and, besides showing atrophy of the cerebellum and marked corpus callosum hypoplasia, T2* relaxation weighted images confirmed that the hypointense T2 and FLAIR weighted areas corresponded to iron increase for age. In VN_X3359, electroencephalography showed bilateral epileptiform interictal abnormalities over the temporal lobes. Seizures were partially controlled under levetiracetam and phenobarbital.

Overall, these data confirm that all individuals suffer from progressive motor neuronopathy and spastic ataxia bearing similarities with the phenotype of the *pmn/pmn* mice. Surprisingly, follow-up MRIs performed in the second decade, particularly in VN_X3359 and VN_X5360, showed a pattern of neurodegeneration with brain iron accumulation (NBIA).

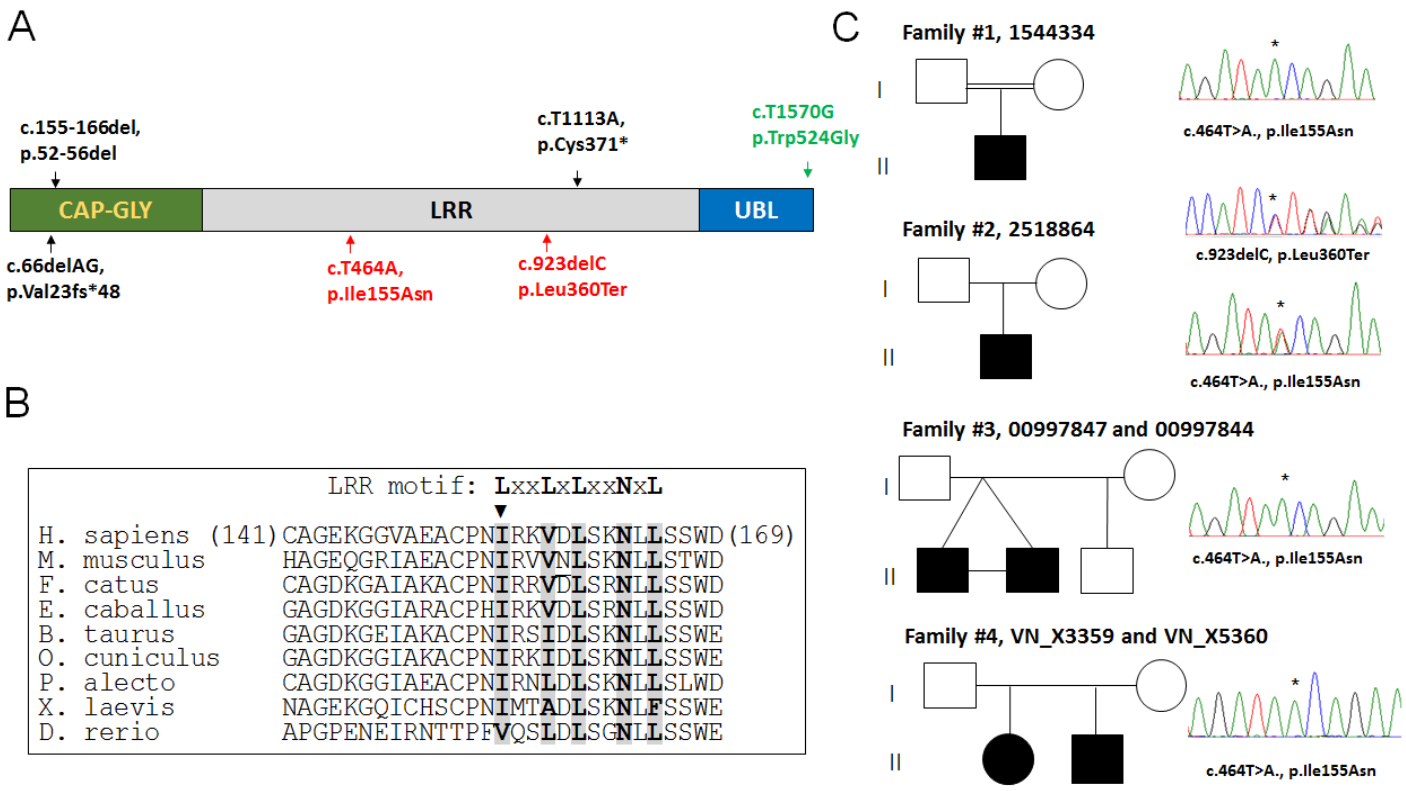

Figure S1. TBCE domain organization, *TBCE* mutations causing early-onset progressive encephalopathy with distal spinal muscular atrophy, and conservation of Ile^{155}.
(**A**) Schematic representation of TBCE and location of known disease-causing mutations. Mutations causing hypoparathyroidism-retardation-dysmorphism (HRD) and Kenny-Caffey syndrome (KCS) are shown in black, while those implicated in neurodegeneration are in red (present study) and green (*pmn*/*pmn* mouse).
(**B**) Multiple sequence alignment of TBCE orthologs. Ile^{155} is indicated (closed triangle). Columns corresponding to the consensus 'L/I' and 'N' residues in the LxxLxLxxNxL motif are highlighted in gray.
(**C**) Pedigrees of the 4 families and chromatograms of the relevant *TBCE* coding sequence showing the disease-associated mutation(s). The location of mutations are shown (asterisk) together with the nucleotide and amino acid changes. *TBCE* mutations are annotated according to the human sequence GenBank accession NM_001079515.2 and NP_001072983.1.

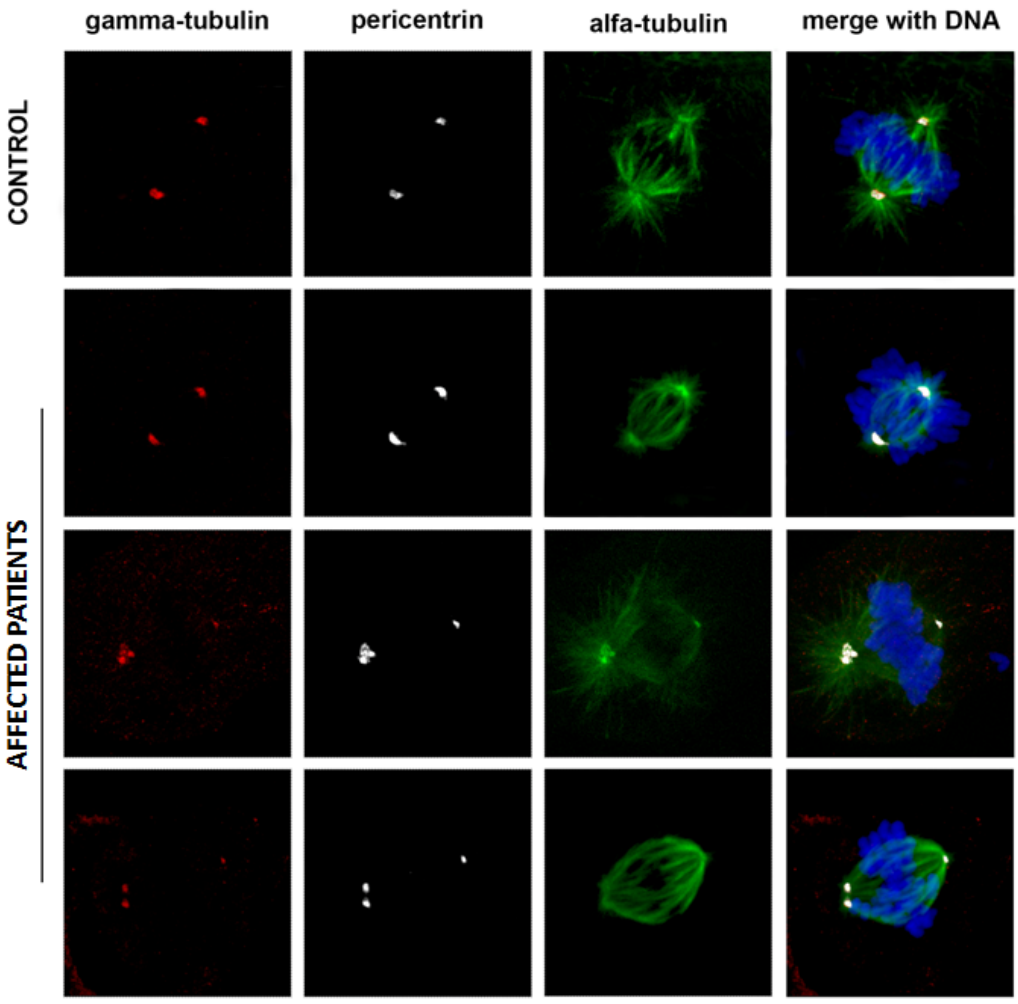

Figure S2. Confocal laser scanning microscopy (CLSM) observations of patient fibroblasts documenting an anomalous mitotic spindle organization.
CLSM analysis performed in synchronized skin fibroblasts from subjects with biallelic *TBCE* mutations show abnormal structures of the mitotic spindle during metaphase. Note the enhanced pericentrin signal, reduced aster formation, asymmetry of spindle and multispot of pericentrin and γ-tubulin compared to control cells. Fibroblasts were stained with pericentrin (grey), γ-tubulin (red), as centrosome markers, and α-tubulin (green) as a marker for microtubules and the mitotic spindle; chromosomes are DAPI stained (blue). Representative images obtained from fibroblasts of subjects 1544334 and 2518864 are shown. Scale bars, 5 μm.

Table S1. Whole exome sequencing data output.

	Family 1	Family 2	Family 3
Target regions coverage, 2x[1]	98.8%	98.7%	98.2%
Target regions coverage, 10x[1]	96.6%	97.2%	96.6%
Target regions coverage, 20x[1]	89.6%	93.7%	93.3%
Average sequencing depth on target[1]	56x	77x	110x
Number of variants with predicted functional effect	13,580	13,631	11,531
Novel, clinically associated, and unknown/low frequency variants[2]	346	346	237
Putative disease genes (autosomal recessive/X-linked trait)	12[3]	12[4]	5[5]
Shared candidate genes (autosomal recessive/X-linked trait)[6]	1, *TBCE*	1,*TBCE*	1, *TBCE*
Genes with putative *de novo* variants	2[7]	3[8]	5[9]
Shared genes with putative *de novo* variants[6]	-	-	-

[1]Referred to SureSelect Human All Exon V.4 (Families 1 and 2) and Agilent Clinical Research Exome (Family 3).

[2]MAF <0.1% in dbSNP144 and ExAC V. 0.3 databases, and with frequency <2% in our *in-house* database.

[3]*AR* (c.228_239dupGCAGCAGCAGCA, p.Gln77_Gln80dup), *ATXN1* (c.672_674dupGCA, p.Gln225dup), *CXorf21* (c.223C>A, p.His75Asn), *FUCA2* (c.-163C>T), *GFI1* (c.925-12_925-5delCTCTCTCT), *IGSF1* (c.877C>T, p.His293Tyr), *NBPF8* (c.1111G>T, p.Ala371Ser), *TBCE* (c.464T>A, p.Ile155Asn), *TRAK1* (c.2090_2095dupAGGAGG, p.Glu697_Glu698dup), *TRO* (c.2462C>T, p.Ala821Val), *ZBTB33* (c.740A>G, p.Gln247Arg), *ZNF469* (c.1409C>G, p.Pro470Arg; c.8701G>A, p.Glu2901Lys).

[4]*BCL2L11* (c.-208C>T), *CCDC150* (c.697T>G, p.Ser233Ala; c.3122G>A, p.Gly1041Asp), *FAM47B* (c.1687A>C, p.Ser563Arg), *GVQW2* (c.159-6delT), *NHS* (c.4127A>G, p.Gln1376Arg), *NOP9* (c.504_509dupGGAGGA, p.Glu168_Glu169dup), *PPP4R4* (c.2373T>G, p.Cys791Trp), RBMXL3 (c.1191_1192insAACGCCCACAGCGGAGGCCGCTCACCC, p.Pro397_Asp398insAsnAlaHisSerGlyGlyArgSerPro), *SPTB* (c.371A>G, p.Lys124Arg; c.964A>G, p.Ile322Val), *TBCE* (c.464T>A, p.Ile155Asn; c.1076delC, p.Ser360Ter), *USF3* (c.4404_4409dupGCAGCA, p.Gln1469_Gln1470dup), *ZDHHC11* (c.1059-8C>G).

[5]*BAHCC1* (c.1070C>T, p.Ala357Val; c.6838G>A, p.Gly2280Ser), *SEC14L5* (c.740T>C, p.Ile247Thr; c.1981_1984dupGGCT, p.Ser662fs), *ST8SIA2* (c.843-17_843-5dupTTTTTTTTTTTTT), *TBCE* (c.464T>A, p.Ile155Asn), *TTN* (c.42904G>A, p.Asp14302Asn; c.81038G>A, p.Arg27013Gln; c.91307G>A, p.Arg30436Gln)

[6]Filtering retained functionally relevant variants (excluding variants predicted as benign by CADD and metaSVM algorithms) in all affected subjects.

[7]*DCHS2* (c.7513G>A, p.Ala2505Thr); *DOCK2* (c.3375C>A, p.Phe1125Leu).

[8]*C17orf77* (c.653G>A, p.Arg218Lys), *HRCT1* (c.299_310dupTCCACCACCACC, p.Leu100_His103dup), *PTGES3L* (c.562-8G>C).

[9]*CARD10* (c.2864+7T>G); *CD40* (c.647-5_647-3dupTTT); *CNTNAP3B* (c.743-4dupT); *SERTAD4* (c.-17-8C>G); *TNN* (c.3760-6delT).

Table S2. Haplotype analysis of the genomic region flanking the c.464T>A change. Haplotypes referred to seven informative SNP/STR markers encompassing the *TBCE* gene documenting a 0.5 Mbp genomic region shared by all chromosomes carrying the c.464T>A change. Recombination was demonstrated at markers STR-1 and ST5-5, indicating that the genomic stretch defining the shared haplotype is < 1.0 Mbp. The haplotype referred to the chromosome bearing the c.1076delC in subject 2518864 is also shown (blue).

Marker/mutation[a]	Subjects									
	1544334		2518864[b]		VN X3359		VN X3360		00997847[c]	
STR-1 (chr1:234,859,467)	156	169	156	156	169	169	169	169	169	169
STR-2 (chr1:235,268,140)	360	360	360	366	360	360	360	360	360	360
D1S2649 (chr1:235,378,863)	431	431	431	442	431	431	431	431	431	431
rs780472451[d] (chr1:235,590,458)	A	A	A	T	A	A	A	A	A	A
rs750781063[e] (chr1:235,599,883)	C	C	C	-	C	C	C	C	C	C
STR-3 (chr1:235,638,265)	174	174	174	170	174	174	174	174	174	174
rs35346732 (chr1:235,715,532)	A	A	A	G	A	A	A	A	A	A
STR-4 (chr1:235,763,717)	316	316	316	324	316	316	316	316	316	316
STR-5 (chr1:235,829,526)	221	221	221	223	221	221	221	221	221	213

[a]Location is referred to hg19.

[b]This subject is compound heterozygote for the c.464T>A (p.Ile155Asn) and c.1076delC (p.Leu360Ter) changes.

[c]Haplotype shared with subject 00997844.

[d]c.464T>A (p.Ile155Asn), 0.0000082 (ExAC)

[e]c.1076delC (p.Leu360Ter), 0.00002 (ExAC)